Moroccan Journal of Chemistry
ISSN: 2351-812X
http://revues.imist.ma/?journal=morjchem&page=login
Assaoui & al. / Mor. J. Chem. 8 N°4 (2020) 1033-1047

Study of the adsorption of fluoride in aqueous solution by eco-friendly cost-effective adsorbent: characterization and adsorption mechanism.

J. Assaoui[(a, *)], A. Kheribech[(a)], L. Khamliche [(b)], R. Brahmi [(c)], Z. Hatim[(a)]

(a) Laboratory of Water and Environment, Department of Chemistry (LEE), Faculty of Sciences, University Chouaïb Doukkali, BP 20, 24000 El Jadida, Morocco
(b) Laboratory of Organic Chemistry, Bioorganic and Environment, Department of Chemistry, Faculty of Sciences, University Chouaïb Doukkali, BP 20, 24000 El Jadida, Morocco
(c) Laboratory of Coordination and Analytical Chemistry (LCCA) Department of Chemistry, Faculty of Sciences, University of Chouaïb Doukkali, BP 20, 24000 El Jadida, Morocco.

** Corresponding author:*
Jihane Assaoui
assaoui.j@ucd.ac.ma
Received 1 Aug 2020,
Revised 14 Sept 2020,
Accepted 15 sept 2020

Abstract

Adsorption potential of Moroccan sodium bentonite clay was investigated for aqueous solution defluoridation using batch equilibrium experiments. The aim of this study was to evaluate the adsorption potential of the natural sodium bentonite clay for fluoride removal from aqueous solution and to explore the mechanism that might occur in the fluoride adsorption process. The compositional, structural and textural characteristics of the natural sodium bentonite clay were determined using accurate physicochemical and mineralogical characterizations. The contents of fluoride ions in aqueous solution were determined by the potentiometric method with a fluoride-specific ion electrode connected to a digital ion analyzer. The study and optimization of various operational parameters such as contact time, initial fluoride concentration, adsorbent dose and initial pH solution were carried out through batch adsorption experiments, conducted at room temperature. The experiments results showed that 30 min of contact time was sufficient for attaining equilibrium between the liquid and solid phases. The maximum aqueous solution defluoridation was noted to be 52.2% in the acidic conditions, and for 5 mg L^{-1} and 2 g L^{-1} of initial fluoride concentration and adsorbent dose, respectively. The experimental data followed pseudo-second-order and fitted well into Freundlich adsorption, indicating multilayer adsorption with heterogeneous energetic distribution of active sites.

Keywords: Defluoridation; aqueous solution; sodium bentonite clay; Batch experiments; Adsorption.

1. Introduction

The discharge of wastewater from various industrial activities containing pollutants such as fluorine into surface water would lead to pollution of groundwater [1] by infiltration-percolation through the ground, which can cause harmful effects on human health and environment. The presence of ion fluoride (F^-) in water has been acknowledged as a major environmental problem worldwide [1] and has become a matter of great concern due to its chronic human carcinogenic behavior [2, 3]. Naturally, the release of fluoride into groundwater resources occurs through the leaching of rocks containing hazardous pollutants supplemented with fluoride [4, 5]. Some industries (e.g. semiconductor manufacturing, glass and ceramic production, aluminium manufacturing industry, fertilizer, …) use compounds containing fluoride for leaching and cleaning process, giving rise to high fluoride concentrations in their wastewater [6], ranging from ten to thousands of mg L^{-1} comparing to natural waters [7], imposing a serious threat to human health [8, 9]. The discharge of industrial wastewater containing F^- into the surface water would lead to groundwater pollution [10]. Groundwater can be considered as one of the important sources of drinking water [11, 12]. Thus, the consumption of this latter can be considered as the major path of human exposure [13, 14, 15]. High fluoride concentration in drinking water may cause dental or skeletal disorder [16, 17], viz, osteoporosis, arthritis, and cancer [3, 18]. The World Health Organization (WHO) classifies the fluoride, as one of the pollutants of water for human consumption. According to this specialized agency, the maximum acceptable F^- concentration in drinking water must not exceed 1.5 mg L^{-1} [19, 20]. Because of the high toxicity of fluoride [21], industrial wastewater containing such as a pollutant is strictly regulated worldwide. Different technologies for defluoridation of wastewater have been investigated to conquer the hazardous impacts of fluoride on the environment and human health. Defluoridation can be achieved by physicochemical and biological methods [22]. Most of physicochemical methods are based on electrocoagulation–flotation [23, 24], membrane separation processes (reverse osmosis, nanofiltration, electrodialysis [25, 26, 27, 28], fluidized-bed precipitation [29], ion exchange [27, 30], electrochemical methods [27] and adsorption techniques [31, 32]. Adsorption has been proved to be a robust and an effective technology for industrial wastewater treatment [33, 34, 35]. Several adsorbents for defluoridation have been described in literature, such as activated carbon derived from various biomass resources [36], zeolites [37] and aluminium based adsorbent [38,39], but research is warranted to discover alternative adsorbents, such as clay and clay minerals, abundantly present in nature and eco-friendly, renewable and environmentally sustainable [40]. Montmorillonite [41, 42], serpentine minerals [43, 44, 45], kaolinite [46, 47] and palygorskite-sepiolite [48] are some of the many classes of clays existing in nature which have been used for wastewater defluoridation. The negative charge on minerals structure is the origin of their adsorption capacity [49]. The adsorption properties of clay also come from their porosity and high surface area [50]. Some of these clays are characterized by a large specific surface area, chemical and mechanical stability, layered structure, high cation exchange capacity, which have made some of those mineral clays as an excellent adsorbent material [51]. Recently, there has been an increasing interest in exploiting clay minerals like sodium bentonite [52, 53], a naturally occurring clay mineral which consists mainly of montmorillonite and quartz. It is becoming a substitute for the use of expensive materials as adsorbent, because of its availability, relatively low-cost, eco-friendly and high adsorption capacity [54, 55]. The work reported here deals with an investigation into the use of locally available sodium bentonite clay (SBC) obtained from a deposit in the northern part of Morocco, it is a clay dune. SBC samples have been tested in their natural state for removal fluoride in aqueous solution based on actual fluorine concentrations in wastewater, to improve naturally the fluoride adsorption efficiency by optimizing the operational parameters such as contact time, initial fluoride concentration, adsorbent dose and pH solution. The characterization of the substrate SBC after defluoridation has never been examined in our knowledge. For

this purpose, physicochemical and mineralogical characterizations were carried out to explore the mechanisms which might probably be involved in the fluoride adsorption process.

2. Experimental works

2.1. Materials

SBC from Northern part of Morocco. All the chemicals used in the present study were of analytical reagent grade. Sodium fluoride (NaF), hydrochloric acid (HCl), caustic soda (NaOH) and TISAB III were purchased from Merck (Germany).

2.2. Purification of Sodium Bentonite Clay

The SBC as dispersed in a volume of water with a ratio solid/liquid 1/5, the solution is stirred until complete homogenization of the suspension we recover 2/3 of the clay in this solution to centrifuge and dry the solid obtained is dried crushed and sieved [51].

2.3. Swelling index

To define the clays characteristics, it is always necessary to determine the swelling index which is considered as one of the parameters characterizing the clay structures. This parameter occurs gradually depending on the evolution of saturation in the clay structure along with the depth of the layer and it should be noted that the interfoliar swelling occurs after interparticle swelling. In the swelling phenomena, the water enters the clay structure through the creation of an interstices lattice, which increases the spaciousness index. The volume deformation depends relatively on the amount of swelling clay. Clays adsorb a significant amount of water due to the attraction force applied on the water molecule by the negative surface of these clays. Some studies carried out in the field of adsorption have reported that the swelling index plays a decisive role in the choice of adsorbent clays and that the higher the swelling index, the greater the adsorption capacity [56]. For this study, the swelling test was carried out following the standardized method ASTM D5890 [57], which consists of filling a 100 mL measuring cylinder with 50 mL of desionised water to which 0.5 g of clay is added. After 45 min, 0.5 g of clay is added to the solution. After 24 h, the swelling volume is noted to determine the swelling index (I_S) according to Eq. (1)

$$I_s\ (\%) = \frac{\text{Swelling volume (Vg)} * 50}{50 - \text{Humidity (H)}} \qquad (1)$$

Where: H is the humidity calculated from the ratio of the mass of water to the mass of solid particles Eq. (2).

$$\mathrm{H}(\%) = \frac{\mathrm{m_{water}}}{\mathrm{m_d}} * 100 = (\mathrm{m_t} - \mathrm{m}_d) * 100 \qquad (2)$$

The obtained value for the SBC swelling index is 0.076 (7.6%) [58] which means that the swelling rate in the clay sites in SBC is medium to high (> 5%) [58] and makes it possible to predict the good adsorption properties of this clay.

2.4. Characterization of adsorbent

The physicochemical and mineralogical characteristics of the SBC were performed by X-Ray Diffraction (XRD X'Pert PRO PANALATYCAL) and X-Ray Fluorescence (XRF, OXFORDMDX 1000). The Specific Surface Area was determined by the BET method using N_2 adsorption (SSA_{N2BET}) (FLOWSORB II 2300, Micromeritics). Energy Dispersive X-ray attached to Scanning Electron Microscopy (SEM-EDX) was used to observe the morphological features of raw and used SBC (samples after defluoridation) and to determine the spot element analysis of these latter. In order to confirm the functional groups present in raw and used Sodium Bentonite Clay, Fourier Transform Infrared (FTIR Bruker VERTEX 70) with a resolution of 4 cm^{-1} where the band range varies from 500 cm^{-1} to 4000 cm^{-1} were recorded on FTIR spectrometer.

2.5. Analytical measurement of fluoride concentration

Sodium fluoride (NaF) was used during adsorption experiments as the source of F^-. A stock solution of 100 mg L^{-1} F^- was prepared by dissolving 221 mg of NaF in 1000 mL of deionized water. Experimental solutions for various experiments were then prepared by appropriate dilution of the stock solution. F^- concentration was measured by the potentiometric method [59] with a fluoride-specific ion electrode (WTW F800 Fluoride Combination Electrode) connected to a digital ion analyzer (WTW InoLab pH/Ion 7320). The use of Total Ionic Strength Adjustment Buffer III (TISAB III) was for maintaining the ionic strength pH constant to decomplex Metal–F complexes present in the sample during measurement [59]. All adsorption experiments were conducted at room temperature of 25±2 °C.

2.6. Adsorption studies through batch experiments

The kinetic parameters of the process consisted in analysing the effect of controlling parameters such as contact time, initial F^- concentration, adsorbent dose and initial pH solution on F^- adsorption onto Sodium Bentonite Clay. All the experiments were conducted at room temperature of 25±2 °C in 500 mL plexiglass reactor. A specific amount of Sodium Bentonite Clay was added to fluoride-doped synthetic solution. The reaction mixture was continuously blended by an electric rod stirrer at 250 rpm. At equilibrium, the liquid phase is recovered in an Erlenmeyer flask after vacuum filtration through Whatman No. 42 filter paper for F^- analysis, while the solid phase is recovered for physicochemical and mineralogical characterization.

2.7. Fluoride removal calculation

The specific amount of the adsorbed F^-,Q_e (mg g^{-1}), was calculated according to Eq. 3:

$$Q_e = \frac{C_0 - C_e}{W} \times V \qquad (3)$$

where, Q_e is the adsorption capacity (mg g^{-1}) in the solid at equilibrium; C_o, C_e are initial and equilibrium concentrations of F^- (mg L^{-1}), respectively; V is the volume of the aqueous solution (L) and W is the mass (g) of adsorbent used in the experiments.

The adsorption removal efficiency (*ARE*), at equilibrium, was calculated by using Eq. 4:

$$ARE\ (\%) = \frac{C_0 - C_e}{C_0} \times 100 \qquad (4)$$

3. Results and discussion

3.1. Characterization of adsorbent

3.1.1. X-Ray Diffraction (XRD) analysis

The structural characterization of Sodium Bentonite Clay was carried out by X-Ray Diffraction (XRD) as shown in Figure 1. XRD pattern of Sodium Bentonite Clay showed that the material consisted mainly of Albite low [Na($AlSi_3O_8$)], Quartz [SiO_2] Sodium Zinc Orthosilicate [$Na_2Zn_3(SiO_4)_2$] and Montmorillonite [$(Na, Ca)_{0.3}$ $(Al, Mg)_2$ $Si_4O_{10}(OH)_2.xH_2O$]. The diffraction pattern was found to be typical for layered structure clays. Furthermore, the Sodium Bentonite Clay was classified as Na-bentonite due to its mineralogical composition.

3.1.2. X-Ray Fluorescence (XRF) analysis

The compositional analysis was carried out to find the chemical composition of the raw Sodium, the analysis revealed that silica (SiO_2) was the main component at 45%, followed by alumina (Al_2O_3) at 23%, confirming that Sodium Bentonite Clay is an alumino-silicate material. The relatively high concentrations of MgO, Na_2O and CaO may probably result in the formation of Metal–F complex after F^- adsorption. This hypothesis will be confirmed in the following characterizations of the raw adsorbent.

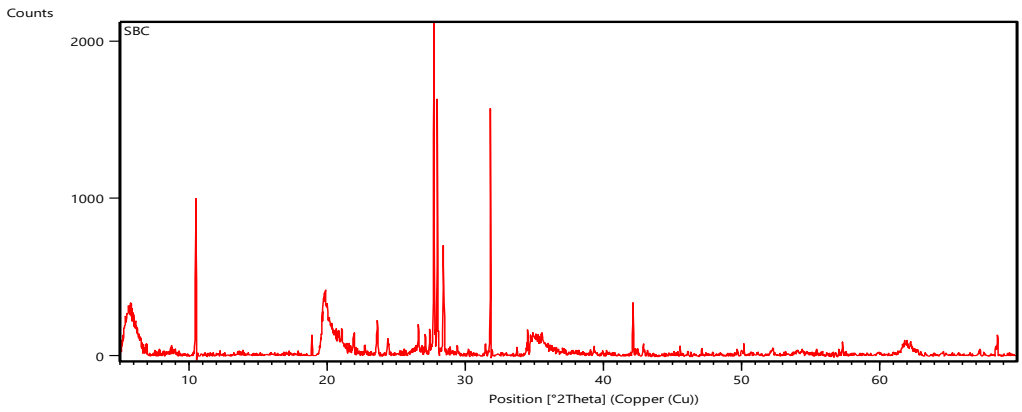

Figure 1. XRD patterns of SBC.

3.1.3. BET Specific Surface Area (SSA_{N2BET}) analysis

The BET surface areas have a pivotal role in the adsorption of chemical substances from the solution. The BET-N_2 determined surface areas (micropore area and external surface area) and micropore volumes of the adsorbent. According to the results, SBC presents a relatively high surface area ($\simeq$ 60 m^2 g^{-1}) comparing to the most of Na-dominated bentonites which have a specific surface area values < 40 m^2 g^{-1} with some exceptions [60]. The value of SSA_{N2BET} indicated that our material is characterized by an important physical property in terms of the F^- adsorption capacity compared to natural bentonites usually reported in the literature for aqueous solution defluoridation [60].

3.1.4. Scanning Electron Microscopy (SEM)

The results of SEM analysis of raw SBC presented in Figure 2 and showed the aspect of the particules are irregular and they have never true isolated crystals but are more lake granular assemblies of silicates layers, they look like paper sheets torn into smaller pieces

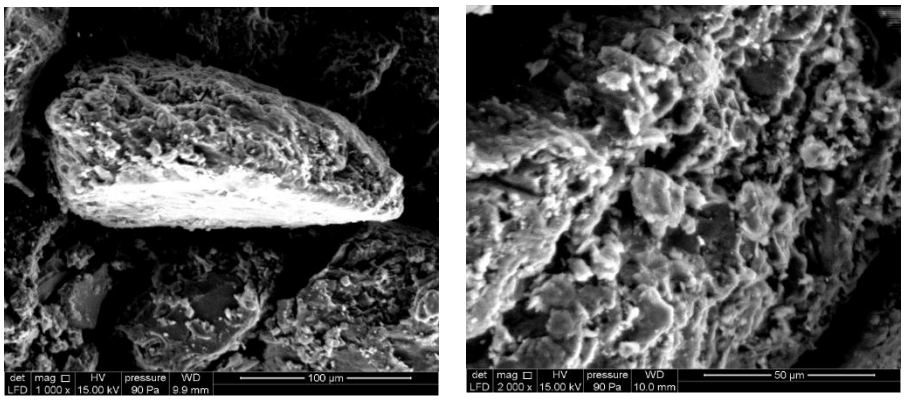

Figure 2. SEM analysis of raw SBC

3.1.5. Fourier-Transform Infrared Spectrometry (FTIR) analysis

FTIR analysis was carried out to determine the functional groups of SBC and to help understand the adsorption mechanism. Figure 3 shows the FTIR spectra of raw and used SBC recorded in the region of 400 – 4000 cm^{-1}. The analysis results show three main absorption regions: 3000 – 3800 cm^{-1}, 1500 – 1800 cm^{-1} and 400 – 1200 cm^{-1}. Those absorbance regions were found in concordance with those obtained by Yang et al. [61] in SBC suspensions. A notable difference was observed in those regions in raw and used Sodium bentonite clay. The spectral band at 3618.10 cm^{-1}

reflects the O–H stretching vibration of the silanol (Si–OH) groups from the solid and the broad band at 3440.70 cm^{-1} may be attributed to H–OH vibration of the water molecules adsorbed on the solid surface. The spectral band at 1643.12 cm^{-1} reflects the bending of H–OH bond of water molecules. The peak at 1118.60 cm^{-1} is corresponded to Si–O vibration. The IR peaks at 918.01 and 524.60 cm^{-1} may be attributed to stretching and vibration of Al–OH–Al and Al–O–Si bending vibrations, respectively. After defluoridation process, it has been observed variations in the intensity of transmittance in all the peaks (consisting most of them of OH groups), which indicates F^- adsorption onto SBC. Since OH and F^- ions have very similar dimensions, they can replace each other (ion exchange) in such way that Metal–F complexes can be formed by the interaction of fluoride and hydroxide ions with metal ions.

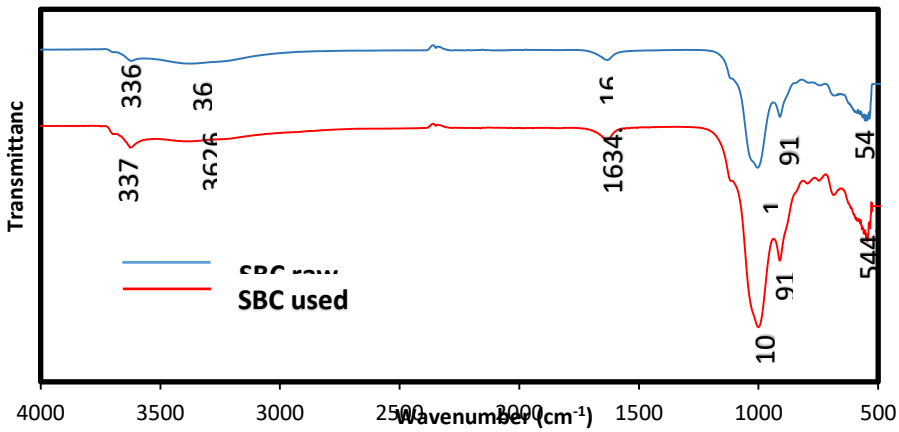

Figure 3. FTIR spectra of raw and used SBC samples.

3.2. Batch experiments results

3.2.1. Effect of contact time

The effect of contact time on the percentage of F^- adsorbed (%) was investigated to ensure equilibrium state between aqueous F^- and the adsorbent. Figure 4 shows the progression of adsorption reaction, the percentage of the F^- adsorbed onto the adsorbent after different contact times. It was observed that with a fixed amount of the adsorbent, the percentage of F^- adsorbed (%) increased with contact time and began to reach equilibrium after 30 min of reaction. Consequently, the period of contact time fixed for further adsorption experiments was 30 min

Table 1. Evolution of the rate of F-adsorbed ions as a function of time.

***t* (min)**	**10**	**30**	**60**	**120**	**180**	**240**	**300**
Q_t (mg.g^{-1})	0,426	0,885	0,885	0,890	0,895	0,897	0,900
% F^- adsorbé	47,39	98,33	98,33	98,89	99,44	99,72	100

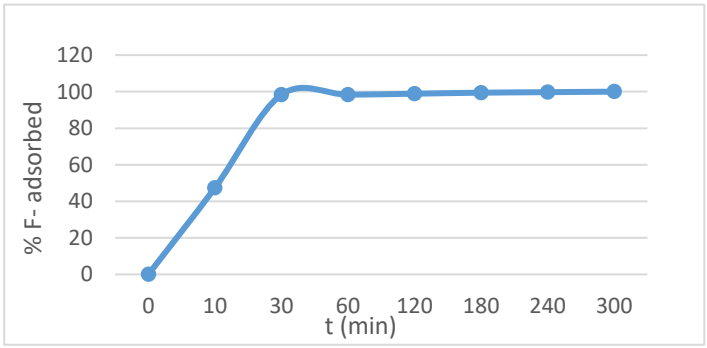

Figure 4. Effect of contact time on the percentage of F^- adsorbed (%).

3.2.2. Effect of initial fluoride concentration

The effect of initial concentration on the percentage of F^- removal was carried out to determine the maximum adsorption capacity of SBC. Six initial F^- concentrations were chosen: 5, 10, 20, 40, 80 and 100 mg L^{-1}. The adsorbent dose and initial pH solution were fixed at 2 g L^{-1} and 5.6±0.2 (natural pH) respectively. As shown in Figure 5, the adsorption capacity . (4.40 mg g^{-1}) reached stability at a high initial concentration (100 mg L^{-1}). This can be explained by saturation of the available active adsorption sites. Although, the percentage of F^- removal decreased with an increase in the initial concentration. This decrease is due to the presence of more F^- ion in solution at higher initial F^- concentration. However, the efficient F^- removal at a low initial concentration was because of important ratio of surface active sites to F^- ions present in solution.

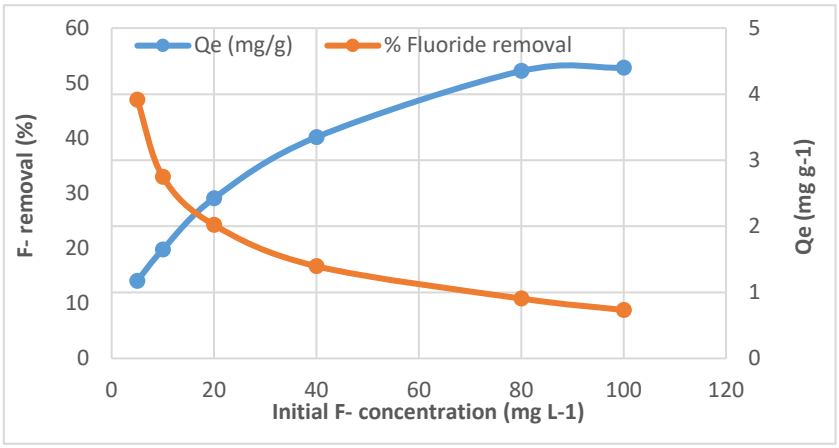

Figure 5. F^- removal and adsorption capacity against initial F^- concentration (natural pH 5.6±0.2, contact time = 30 min, adsorbent dose = 2 g L^{-1}, agitation speed = 250 rpm, T = 25±2 °C).

3.2.3. Effect of adsorbent dose

The effect of adsorbent dose on F^- removal (%) was determined for 5 mg L^{-1} initial F^- concentration at natural pH 5.6±0.2. The tested adsorbent doses varied from 2 to 12 g L^{-1} as shown in Figure 6. It was observed that the percentage of F^- removal increased slightly with increasing adsorbent dose up to 8 g L^{-1}. The increase of percent F^- removal with the increase of adsorbent dose is due to the availability of sufficient adsorption sites. However, the addition of the adsorbent dose didn't show any considerable increase in the percentage of F^- removal. This may be probably due to the overlapping phenomenon of the active sites at a higher adsorbent dose resulting in a reduction of surface area.

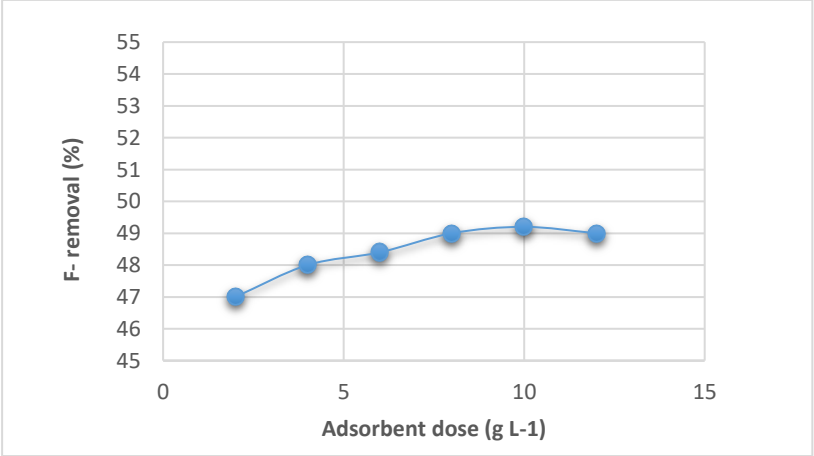

Figure 6. Effect of adsorbent dose on percentage of F^- removal (natural pH = 5.6±0.2, initial F^- concentration = 5 mg L^{-1}, contact time = 30 min, agitation speed = 250 rpm, T = 25±2 °C).

3.2.4. Effect of initial pH solution and determination of pHPZC

The effect of initial pH solution on the F^- removal was carried out in the pH range of 2 – 12. The initial F^- concentration and the adsorbent dose were fixed at 5 mg L^{-1} and 2 g L^{-1} respectively. The pH adjustment was realized by using 0.1 N (HCl) or 0.1 N (NaOH). Figure 7 illustrates the evolution of the percentage of F^- removal over the pH range of 2 – 12. It was observed that as the pH of the initial F^- solution increased from 2 to 12, the percentage of F^- removal by SBC decreased from 52.2 to 20%. This can be explained by the pH dependency of the SBC toward F^- adsorption in the acid conditions, which is in concordance with the results obtained by Srimurali and Bar-Yosef [52, 62]. In the other hand, there were no considerable evolutions in the percentage of F^- removal within a pH range of 4 – 6. Regarding the mechanism involved during aqueous solution defluoridation, it is well known that SBC consists of a mixture of several oxides. The hydroxilated surfaces of these latters develop charge on the surface in a humid environment. Low pH values probably results in the neutralisation of the negative charges developed at the surface of SBC, which may consequently result in the increased adsorption of the negatively charged fluoride ion.

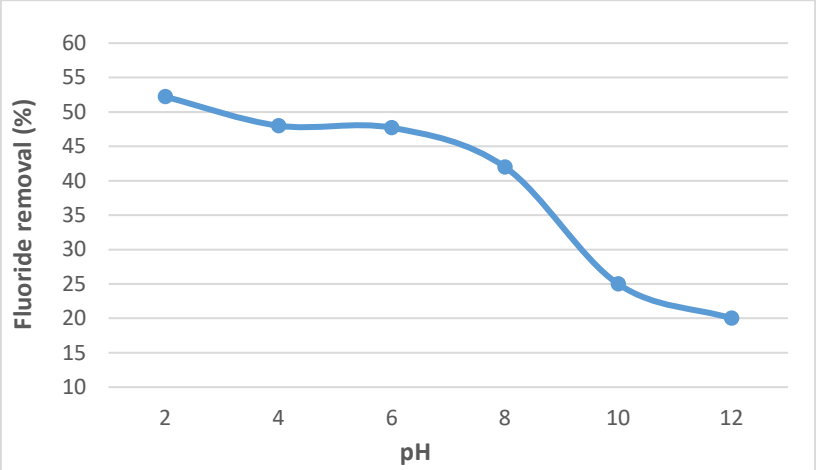

Figure 7. Effect of pH on percentage of F^- removal (adsorbent dose = 2 g L^{-1}, initial F^- concentration = 5 mg L^{-1}, contact time = 30 min, agitation speed = 250 rpm, T = 25±2 °C).

The clays affinity on F^- ions is due to the Lewis and Brönsted acid sites which exist on their surface. Furthermore, the clays' acidity plays a determining role in the definition of the isoelectric point and the point of zero charges (PZC). To identify the optimal pH value where the F^- ions are absorbed by sodium bentonite clay, we determined the point zero charge using drift method [63], by adding 20 mL of NaCl solution (0.05 M) to several cylindrical polystyrene bottles. The initial pH values (pH_i) of the NaCl solutions were adjusted from 2 to 12, by adding solutions of hydrochloric acid (0.1 M HCl) and/or sodium hydroxide (0.1 M NaOH). The total volume of the solution in each bottle was increased to a maximum of 30 mL by a supplementary addition of the NaCl solution. The pH_i values of the solutions were precisely noted before the addition of 50 mg of the adsorbent in the various bottles which were immediately tightly closed. The solutions were stirred magnetically at room temperature for 5 min, and then left to equilibrate for 48 h. The solutions were then centrifuged at 3600 rpm for 15 min and the final pH values (pH_f) of the supernatant were noted. The pH_{PZC} value is theoretically the intersection point of the curve of ΔpH (pH_f - pH_i) as a function of pH_i with the x-axis [64]. The results obtained Figure 8 show that our adsorbent has a point of zero charge equal to 8.7. It should be noted that the adsorption of F^- ions is only favorable when the adsorbents are positively charged at a particular pH. (pHsolution <pH_{PZC}) [63]. Therefore, it can be concluded that the optimal pH of the sodium bentonite clay is between 2 and 8.7 [65, 66], and more particularly under acidic conditions as demonstrated by the pH effect study presented above.

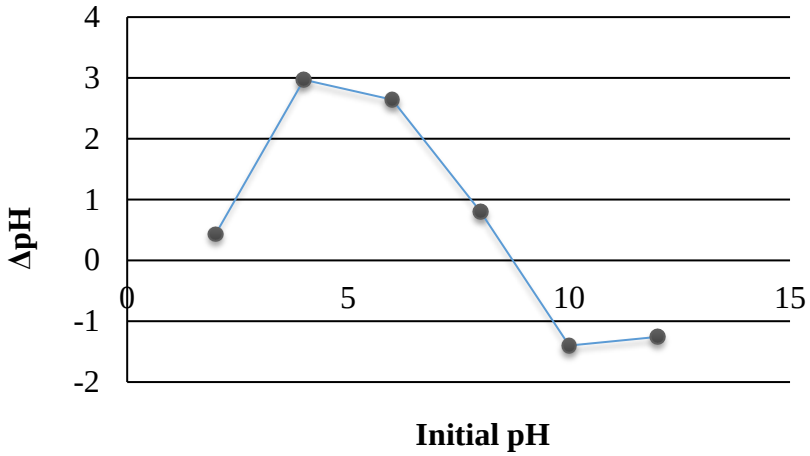

Figure 8. Point of zero charge determination (PH_{PCZ}).of SBC

3.3. Kinetic studies of fluoride on SBC

The adsorption speed is largely influenced by several parameters, mainly the status of the solid matrix and the physicochemical conditions under which the adsorption takes place. The main objective of the study of adsorption kinetics is for understanding the involved mechanism and the rate controlling steps affecting the adsorption kinetics. Several models are exploited to fit the kinetic sorption tests. In this study, the kinetics of F^- adsorption on SBC was verified using pseudo-first order and pseudo-second order, equation. The pseudo first order is a kinetic model described by the following Lagergren Eq. 5 [67]:

$$\frac{dQ_t}{dt} = K_1(Q_e - Q_t) \quad (5)$$

The linear form of pseudo-first order kinetic model can be expressed by Eq. (6):

$$\log(Q_e - Q_t) = \log Q_e - (\frac{K_1}{2.3})\, t \quad (6)$$

where, Q_e and Q_t are the amount of F^- adsorbed (mg g^{-1}) at equilibrium and at time '*t*', respectively. K_1 (min^{-1}) represents the rate constant of pseudo-first order adsorption reaction. A straight line of $\log(Q_e - Q_t)$ against *t* suggests the applicability of these kinetic models. Both Q_e and K_1 can be determined from the intercept and slope of the curve, respectively.

The linear form of pseudo-second order kinetic model can be expressed by Eq. 7 [68]:

$$\frac{t}{Q_t} = \left(\frac{1}{K_2 \times Q_e^2}\right) + \frac{t}{Q_e} \quad (7)$$

where, K_2 is the rate constant for pseudo-second order reaction (g mg^{-1} min^{-1}). Q_e and Q_t are the amounts of F^- adsorbed at equilibrium and at any time '*t*' (mg g^{-1}), respectively. The straight line plot of t/Q_t against *t* for the kinetic data gives the values for Q_e and K_2 from the slope and intercept, respectively. As shown in Figure 9, the pseudo-first order (a) has a very low correlation coefficient ($R^2 \simeq 0.500$). However, the pseudo-second order (b) was found to give the best fit (R^2 = 0.999) and therefore, it could be used to predict the adsorption kinetics of F^- onto SBC.This results leads us to conclude that the adsorption process of F-ions on natural bentonite is well suited to the pseudo-second order model.

Table 2. Coordinates of the linear transform points of the two kinetics studied

***t* (min)**	**10**	**30**	**60**	**120**	**180**	**240**	**300**
Q_t (mg.g^{-1})	0,426	0,885	0,885	0,890	0,895	0,898	0,900
$\log(Q_e-Q_t)$	-0,31	-1,60	-1,60	-1,70	-1,82	-1,90	-2,00
t/Q_t	23,45	33,90	67,80	134,83	201,12	267,41	333,33

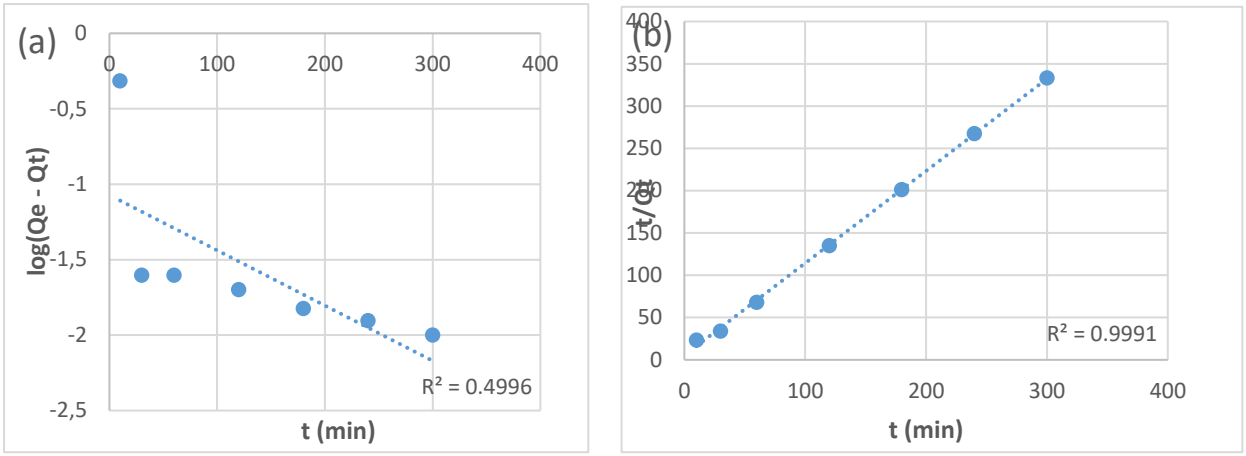

Figure 9. Adsorption kinetics for F^- onto SBC.

3.3. Adsorption isotherm

Adsorption equilibrium is established when the amount of adsorbate in the liquid phase (C_e) is in dynamic balance with that on the liquid–solid interface (Q_e). Therefore, two isotherm equations have been used in the present study, namely Langmuir and Freundlich isotherm models to describe the equilibrium data. The Langmuir model is based on the hypothesis that uptake occurs on a homogenous surface by monolayer adsorption without interaction between adsorbed molecules. The Langmuir equation can be described in the following Eq. 8 [69]:

$$Q_e = \frac{Q_m \times K_L \times C_e}{1 + (K_L \times C_e)} \quad (8)$$

The linearized form of Eq. (6) can be written as Eq. 9:

$$\frac{1}{Q_e} = \left(\frac{1}{Q_m \times K_L}\right)\left(\frac{1}{C_e}\right) + \frac{1}{Q_m} \quad (9)$$

where, C_e is the equilibrium concentration of fluoride ions (mg L^{-1}), Q_e is a solid phase concentration of fluoride ions (mg g^{-1}), Q_m (mg g^{-1}), and K_L (L mg^{-1}) are empirical constants, can be evaluated from the slope and intercept of the linear plot of $1/Q_e$ against $1/C_e$.

The Freundlich model proposes a multilayer adsorption with a heterogeneous energetic distribution of active sites and with the interaction between adsorbed molecules. It is expressed mathematically in linear form as it is represented in Eq. 10 [70].

$$\log Q_e = \log K_F + \frac{1}{n} \log C_e \quad (10)$$

where, K_F (mg g^{-1}) and $1/n$ are Freundlich constants related to adsorption capacity and adsorption intensity, respectively. Those constants are obtained from the intercept and slope of $\log Q_e$ versus $\log C_e$ linear plot respectively. The adsorption capacity Q_e (mg g^{-1}) of SBC was examined by determining equilibrium sorption of F^- as a function of residual F^- concentration present in the liquid phase. The variation of the adsorption capacity of SBC for F^- is presented in Figure 10. According to the equilibrium curve, the adsorption capacity at equilibrium increases progressively at lower F^- concentration. This is because of the availability of excess adsorption sites. On the other hand, as the F^- concentration increases, the adsorption capacity at equilibrium progressively decreases until reaching saturation. The availability of adsorption sites at high F^- concentration becomes the limiting factor as the adsorbent surface reaches maximum adsorption capacity. This latter was observed to be 4.40 mg g^{-1}. The equilibrium data was further processed using Langmuir and Freundlich isotherms. The Langmuir and Freundlich adsorption isotherms for the F^- adsorption onto SBC are presented in Figure 11. According to experimental data, it can be observed that Freundlich isotherm. Figure 11 (b) (R^2 = 0.993) better describes the adsorption data than the Langmuir isotherm Figure 11 (a) (R^2 = 0.940). The value of $1/n$ is 0.39 for Freundlich isotherm. Since the value of this constant, $1/n$ (adsorption intensity) is between 0 and 1 ($0 < 1/n < 1$), it indicates a favorable adsorption.

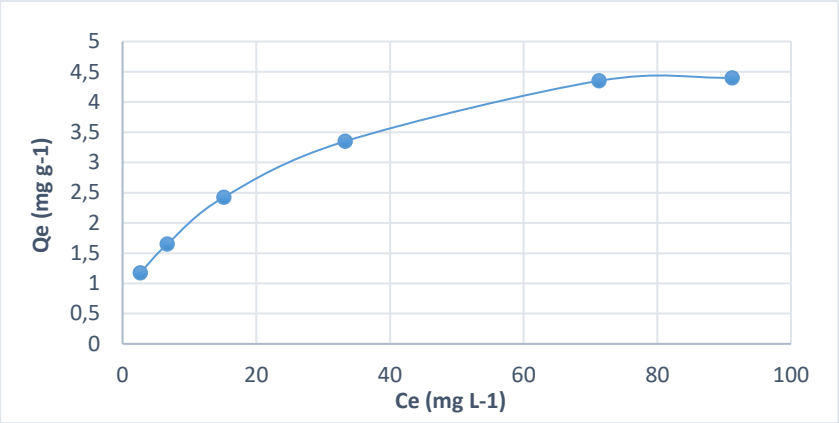

Figure 10. Adsorption isotherm of F^- sorption on SBC (adsorbent dose = 2 g L^{-1}, natural pH = 5.6±0.2, contact time = 30 min, initial concentration 5 – 100 mg L^{-1}, agitation speed = 250 rpm, T = 25±2 °C).

Table 3. Coordinates of the points of linear transforms of the mathematical models of Langmuir and Freundlich

C_0 (mg.L^{-1})	5	10	20	40	80	100
C_e (mg.L^{-1})	2,65	6,7	15,15	33,3	71,3	91,2
Q_e (mg.g^{-1})	1,175	1,65	2,425	3,35	4,35	4,4
$1/C_e$	0,38	0,15	0,07	0,03	0,01	0,01
$1/Q_e$	0,85	0,61	0,41	0,30	0,23	0,23
logC_e	0,42	0,83	1,18	1,52	1,85	1,96
logQ_e	0,07	0,22	0,39	0,52	0,64	0,64

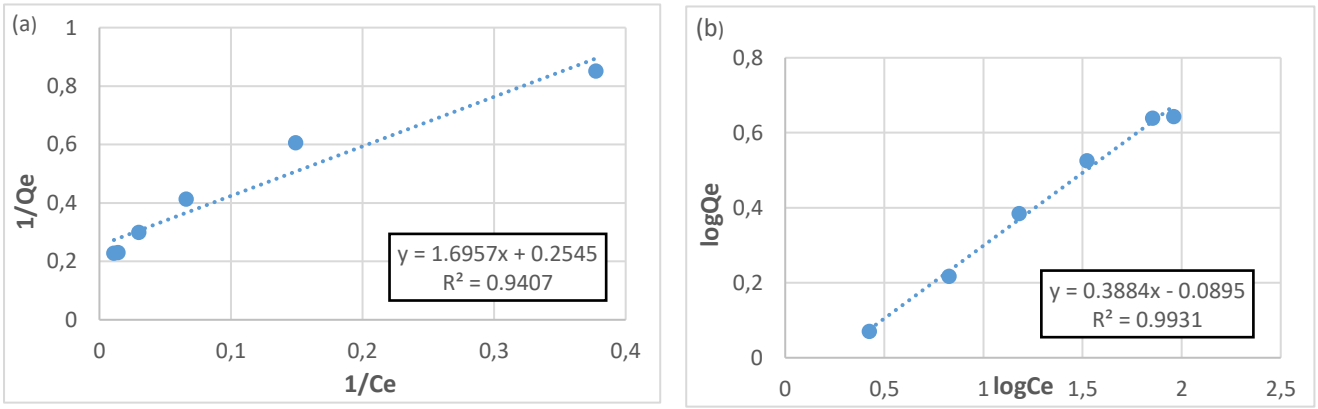

Figure 11. Langmuir (a) and Freundlich (b) isotherm plots for F^- adsorption onto SBC (adsorbent dose = 2 g L^{-1}, natural pH = 5.6±0.2, contact time = 30 min, initial F^- concentration 5 – 100 mg L^{-1}, agitation speed = 250 rpm, T = 25±2 °C). Basing on Freundlich concept, the F^- adsorption system was more likely a multilayer coverage of the SBC with heterogeneous energetic dispersion of active sites and with interaction between adsorbed molecules which concludes that we have a chemisorption.

4. Conclusion

An effective adsorption for fluoride removal aqueous solution of SBC was evaluated in a batch reactor at room temperature (25±2 °C). The results of this study demonstrated that 30 min of contact time between the adsorbent and the aqueous solution r was sufficient to achieve equilibrium. It was observed that the maximum aqueous solution

defluoridation (52.2%) was obtained in the acidic conditions (pH = 2) and for 5 mg L^{-1} and 2 g L^{-1} of initial F^- concentration and adsorbent dose, respectively. Kinetic studies revealed that F^- adsorption fitted well to pseudo-second-order model. Furthermore, the adsorption isotherm of F^- sorption on SBC indicated that the maximum adsorption capacity of this latter was noted to be 4.4 mg g^{-1}. The experimental data indicated that the Freundlich isotherm was the suitable model for describing the F^- adsorption onto SBC because of its high correlation coefficient. According to Freundlich concept, the adsorption of F^- onto SBC was multilayer with heterogeneous distribution of active sites and with interaction between adsorbed molecules. The originality of this paper consisted in introducing the mechanisms that might occur in the F^- adsorption process by physicochemical characterization of raw and used SBC. The obtained results indicated that the ion exchange was probably the main process involved in the F^- adsorption process, accompanied by interactions of fluoride with metal ions. Therefore, the use of SBC as an adsorbent for aqueous solution defluoridation is potentially cost-effective. However, the rest of this work aims to modify the SBC by introducing chemicals which aim to develop a new adsorbent at low cost, having physicochemical properties compatible with fluorine chemistry.

Nomenclature

C_0 Initial F^- concentrations (mg L^{-1})

C_e Equilibrium concentrations of F^- (mg L^{-1})

K_F Freundlich constants related to adsorption capacity (mg g^{-1})

K_1 Pseudo-first order rate constant (min^{-1})

K_2 Pseudo-second order rate constant (g mg^{-1} min^{-1})

n Adsorption intensity (heterogeneity factor)

Q_t Amount of F^- adsorbed per unit mass of adsorbent at time t

Q_e Equilibrium adsorbate capacity (mg g^{-1})

V Volume of the aqueous solution (mL)

W Mass of adsorbent (g)

m_{water} Mass of water

m_s Mass of dry sample (g).

m_t Mass of the wet sample (g).

References

[1] A.K. Tolkou, M. Manassis, I.A. Katsoyiannis, M. Ernst, A.I. Zouboulis, Fluoride removal from water by composite AL/Fe/Si/Mg pre-polymerized coagulants : charactériszation and application, chemosphere., 231, (2019), 528-537

[2] A. Vinati, B. Mahanty, S.K. Behera, Clay and clay minerals for fluoride removal from water: A state-of-the-art review, App. Clay Sci., 114, (2015), 340-348.

[3] A. Bhatnagar, E. Kumar, M. Sillanpaa, Fluoride removal from water by adsorption-A review, Chem. Eng. J., 171, (2011), 811-840.

[4] S.M. Yakout, A.A.M. Daifullah, S.A. Elreefy, Adsorption of fluoride in aqueous solution using $KMnO_4$-modified activated carbon derived from steam pyrolysis of rice straw, J. Hazard. Mater., 147, (2007), 633-643.

[5] S.P. Kamble, P. Dixit, S.S. Rayalu, N.K. Labhsetwar, Magnesium incorporated bentonite clay for defluoridation of drinking water, Desalination, 249, (2009), 687-693.

[6] L. F. Castañeda, O. Coreño, J. L. Nava, G. Carreño, Removal of fluoride and hydrated silica from underground water by electrocoagulation in a flow channel reactor, J. Chemosphere, (2020), 125417.

[7] G. De La Puente, J.J. Pis, J.A. Menendez, P. Grange, Thermal stability of oxygenated functions in activated carbons, J. Anal. Appl. Pyrolysis., 43, (1997), 125-138.
[8] A.K. Chaturvedi, K.P. Yadava, K.C. Pathak, V.N. Singh, Defluorination of water by adsorption on fly ash, Water Air Soil Pollut., 49, (1990), 41-69.
[9] A. Toyoda, T. Taira, A new method for treating fluorine wastewater to reduce sludge and running costs, IEEE Trans. Semicond. Manuf., 13, (2000), 305-309.
[10] F. Shen, X. Chen, P. Gao, G. Chen, Electrochemical removal of fluoride ions from industrial wastewater, Chem. Eng. Sci., 58, (2003), 987-993.
[11] S. Joshi, M. Adhikari, Removal of fluoride ions by adsorption onto Fe_2O_3 /Areca Nut activated carbon composite, J. Inst. Eng., 12, (2016), 175-183.
[12] M. Yousefi, S. Ghalehaskar, F. B. Asghari, A. Ghaderpoury, M. H. Dehghani, M. Ghaderpoori, A. A. Mohammadi, Distribution of fluoride contamination in drinking water resources and health risk assessment using geographic information system, northwest Iran, J. Reg. Toxicol. Pharm., 107, (2019), 104408.
[13] M. Agarwal, K. Rai, R. Shrivastav, S. Dass, Deflouridation of water using amended clay, J. Clean. Prod., 11, (2003), 439-444.
[14] M.G. Sujana, H.K. Pradhan, S. Anand, Studies on sorption of some geomaterials for fluoride removal from aqueous solutions, J. Hazard. Mater., 161, (2009), 120-125.
[15] A. Dhillon, S. Nehra, D. Kumar, Dual adsorption behaviour of fluoride from drinking water on Ca-Zn$(OH)_2CO_3$ adsorbent, J. Surf. In., 6, (2017), 154-161.
[16] T.J. Sorg, Treatment technology to meet the interim primary drinking water regulations for inorganics, J. Am. Water Works Ass., 70, (1978), 105-111.
[17] S. Gao, R. Sun, Z. Wei, H. Zhao, H. Li, F. Hu, Size-dependent defluoridation properties of synthetic hydroxyapatite, J. Fluorine Chem., 130, (2009), 550-556.
[18] E.W. Wambu, C.O. Onindo, W. Ambusso, G.K. Muthakia, Removal of fluoride from aqueous solutions by adsorption using a siliceous mineral of a kenyan origin, Clean Soil Air Water., 41, (2013), 340-348.
[19] WHO, Guidelines for Drinking Water Quality, World Health Organization, Geneva, Vol. 45, (1993).
[20] A. Mekonen, Integrated biological and physiochemical treatment process for nitrate and fluoride removal, Water Res., 35, (2011), 3127-3136.
[21] S. Singha, M. Germanb, S. Chaudharia, A. K. Senguptab, Fluoride removal from groundwater using Zirconium Impregnated Anion Exchange Resin, J. Env. Mang, 263, (2020), 110415.
[22] C.J. Huang, J.C. Liu, Precipitate flotation of fluoride-containing wastewater from a semiconductor manufacturer, Water Res., 33, (1999), 3403-3412.
[23] C.Y. Hu, S.L. Lo, W.H. Kuan, Y.D. Lee, Removal of fluoride from semiconductor wastewater by electrocoagulation–flotation, Water Res., 39, (2005), 895-901.
[24] S. Raghav, M. Nair, D. Kumar, Tetragonal prism shaped Ni-Al bimetallic adsorbent for study of adsorptive removal of fluoride and role of ion-exchange, App Surf Sci., 498, (2019), 14378.
[25] J.N. Pereira, R. Lima, G. Choudhary, P.R. Sharma, S. Ferdov, G. Botelho, R.K. Sharma, S.L. Mendez, Highly efficient removal of fluoride from aqueous media through polymer composite membranes, Sep and Puri Tech., 205, (2018), 1-10.
[26] A.J. Karabelas, S.G. Yiantsios, Z. Metaxiotou, S. Stavroulias, Water and materials recovery from fertilizer industry acidic effluents by membrane processes, Desalination., 138, (2001), 93-102.
[27] P. Miretzky, A.F. Cirelli, Fluoride removal from water by chitosan derivatives and composites: A review, J. Fluorine Chem., 132, (2011), 231-240.

[28] L.S. Thakur, P. Mondal, Simultaneous arsenic and fluoride removal from synthetic and real groundwater by electrocoagulation process: Parametric and cost evaluation, J. Environ. Manage., 190, (2017), 102-112.
[29] R. Aldaco, A. Irabien, P. Luis, Fluidized bed reactor for fluoride removal, Chem. Eng. J., 107, (2005), 113-117.
[30] L. Ruixia, G. Jinlong, T. Hongxiao, Adsorption of fluoride, phosphate, and arsenate ions on a new type of ion exchange fiber, J. Colloid Interface Sci., 248, (2002), 268-274.
[31] M. Yang, M.T. Hashimoto, N. Hoshi, H. Myoga, Fluoride removal in a fixed bed packed with granular calcite, Water Res., 33, (1999), 3395-3402.
[32] Y. Zhou, C. Yu, Y. Shan, Adsorption of fluoride from aqueous solution on La^{3+}-impregnated cross-linked gelatin, Sep. Purif. Technol., 36, (2004), 89-94.
[33] S.S. Tripathy, J.L. Bersillon, K. Gopal, Removal of fluoride from drinking water by adsorption onto alum-impregnated activated alumina, Sep. Purif. Technol., 50, (2006), 310-317.
[34] H. Liu, S. Deng, Z. Li, G. Yu, J. Huang, Preparation of Al–Ce hybrid adsorbent and its application for defluoridation of drinking water, J. Hazard. Mater., 179, (2010), 424-430.
[35] S. Singha, M. Germanb, S. Chaudharia, A. K. Senguptab, Fluoride removal from groundwater using Zirconium Impregnated Anion Exchange Resin, J. Env. Mang, 263, (2020), 110415.
[36] G. Karthikeyan, S. Ilango, Fluoride sorption using Morringa indica-based activated carbon, Iranian J. Environ. Health Sci. Eng., 4, (2007), 21-28.
[37] Y. Sun, Q. Fang, J. Dong, X. Cheng, J. Xu, Removal of fluoride from drinking water by natural stilbite zeolite modified with Fe(III), Desalination., 277, (2011), 121-127.
[38] J. Assaoui, Z. Hatim, A. Kheribech, Synthesis and characterization of aluminum-based adsorbent and application in fluoride removal from aqueous solution, M. J. C., 10(1), (2020), 46-61.
[39] S. Ghorai, K.K. Pant, Equilibrium, kinetics and breakthrough studies for adsorption of fluoride on activated alumina, Sep. Purif. Technol., 42, (2005), 265-271.
[40] R. Srinivasan, Advances in application of natural clay and its composites in removal of biological, organic, and inorganic contaminants from drinking water, Adv. Mater. Sci. Eng., 201, (2011), 1-17.
[41] G. Bia, C.P. De Pauli, L. Borgnino, The role of Fe(III) modified montmorillonite on fluoride mobility: adsorption experiments and competition with phosphate, J. Environ. Manage., 100, (2012), 1-9.
[42] E. Derakhshani, A. Naghizadeh, Optimization of humic acid removal by adsorption onto Bentonite and Montmorillonite nanoparticles, J. Moliq, 03, (2018), 014.
[43] D. Kulkarni, G.W. Nawlakhe, Serpentine – its limitations as a defluoridation medium, Indian J. Environ. Health., 1974, 16, 151-158.
[44] S. Chidambaram, A.L. Ramanathan, S. Vasudevan, Fluoride removal studies in water using natural materials – Technical Note, Water SA., 29, (2003), 339-344.
[45] M. Said, W.T. Rizki, W. Purwaningrum, A. Rachmat, F. Ferlinahayati, P.L. Hariani, Modification bentonite using Fe(III) and its application as adsorbent for phenol, M. J. C., 9(6), (2020), 422-431.
[46] S. Wei, W. Xiang, Surface properties and adsorption characteristics for fluoride of kaolinite, ferrihydrite and kaolinite-ferrihydrite association, J. Food Agric. Environ., 10, (2012), 923-929.
[47] N. Nabbou, M. Belhachemi, M. Boumelik, T. Merzougui, D. Lahcene, Y. Harek, A. Zertpas, M. Jeguirim, Removal of fluoride from gondwater using natural clay (kaolinite): Optimizationof adsorption conditions, Comp rend chi., 22, (2019), 105-112.
[48] Z. Shengyu, L.Ü. Ying, L.I.N. Xueyu, Z. Yuling, S.U. Xiaosi, Performance and mechanisms of fluoride removal from groundwater by lanthanum-aluminum-loaded hydrothermal palygorskite composite, Chem. Res. Chin. Univ., 31, (2015), 144-148.

[49] G. Crini, Non-conventional low-cost adsorbents for dye removal: a review, Bioresour. Technol. 97, (2006), 1061-1085
[50] M. Alkan, Ö. Demirbas, S. Çelikçapa, M. Dogan, Sorption of acid red 57 from aqueous solutions onto sepiolite, J. Hazard. Mater., 116, (2004), 135-145.
[51] W.M. Gitari, T. Ngulube, V. Masindi, J.R. Gumbo, Defluoridation of groundwater using Fe^{3+}-modified bentonite clay: optimization of adsorption conditions, Desalin. Water Treat., 53, (2013), 1578-1590.
[52] M. Srimurali, A. Pragathi, J. Karthikeyan, study on removal of fluorides from drinking water by adsorption onto low-cost materials, Environ. Pollut., 99, (1998), 285-289.
[53] Y. Ma, F. Shi, X. Zheng, J. Ma, C. Gao, Removal of fluoride from aqueous solution using granular acid-treated bentonite (GHB): Batch and column studies, J. Hazard. Mater., 185, (2011), 1073-1080.
[54] M.K. Uddin, A review on the adsorption of heavy metals by clay minerals, with special focus on the past decade, Chem. Eng. J., 308, (2017), 438-462.
[55] K. Chinoune, K. Bentaleb, Z. Bouberka, A. Nadim, U. Maschke, Adsorption of reactive dyes from aqueous solution by dirty bentonite, Ap. C. S., 123, (2016), 64–75
[56] Hassett, J.J., Means, J.C., Sorption properties of sediments and energy-related pollutants. Environmental Research Laboratory, Office of Research and Development, US Environmental Protection Agency., (1980), pp. 125.
[57] ASTM D5890 – 19: Standard test method for swell index of clay mineral component of geosynthetic clay liners., (2019).
[58] Seed, H.B., Lundgren, R., Prediction of swelling potential for compacted clays, Journal of the Soil Mechanics and Foundations Division., 88, (1962), 53-88.
[59] NF T 90-004: Water quality – Determination of fluoride ion – Potentiometric method, (2002).
[60] S. Kaufhold, R. Dohrmann, M. Klinkenberg, S. Siegesmund, K. Ufer, N_2-BET specific surface area of bentonites, J. Colloid Interface Sci., 349, (2010), 275-282.
[61] S. Yang, D. Zhao, H. Zhang, S. Lu, L. Chen, X. Yu, Impact of environmental conditions on the sorption behavior of Pb(II) in Na-bentonite suspensions, J. Hazard. Mater., 183, (2010), 632-640.
[62] B. Bar-Yosef, I. Afik, R. Rosenberg, Fluoride sorption by montmorillonite and kaolinite, Soil Sci., 145, (1988), 194-200.
[63] Sakurai, K., Ohdate, Y., Kyuma, K. Comparison of salt titration and potentiometric titration methods for the determination of zero point of charge (ZPC). Soil Science and Plant Nutrition., 34, (1988), 171-182.
[64] Tan, S.H., Ismail, N.A., Isotherm and kinetic studies of L-Phenylalanine adsorption onto porous nanosilica. Materials Today: Proceedings., 5, (2018), 3193-3201.
[65] D.S. Kim, Mesurement of point of zero charge of bentonite by solubilization technique and its dependence of surface potential on pH. Environ. Eng. Res, 8, (2003), 222-227.
[66] M. Dessalegne,. F. Zewge,.W. Mammo, G. Woldetinsae, I. Diaz, Effective fluoride adsorption by aluminum oxide modified clays: Ethiopian bentonite vs commercial montmorillonite. Bull. Chem. Soc. Ethiop., 32, (2018), 199-211.
[67] K. Bhattacharyya, S. Gupta, Influence of acid activation on adsorption of Ni (II) and Cu (II) on kaolinite and montmorillonite: kinetic and thermodynamic study, Chem. Eng. J., 136, (2008), 1-13.
[68] E.I. Unuabonah, K.O. Adebowale, B.I. Olu-Owolabi, Kinetic and thermodynamic studies of the adsorption of lead (II) ions onto phosphate-modified kaolinite clay. J. Hazard., Mater. 144, (2007), 386-395.
[69] I. Langmuir, The constitution and fundamental properties of solids and liquids, J. Am. Chem. Soc., 38, (1916), 2221-2295.
[70] H.M.F. Freundlich, Over the adsorption in solution, J. Phys. Chem., 57, (1906), 385-470.